

## POST SHOCK HEAT INDUCED BY HIGH-VELOCITY OBLIQUE IMPACTS ON POROUS ICY BODIES.

H. Sasai, M. Aarakawa and M. Yasui, Graduate School of Science, Kobe University (1-1, Rokkodai-cho, Nada-ku, Kobe, 6578501, Japan, 199s408s@stu.kobe-u.ac.jp).

**Introduction:** Comet nuclei may have highly porous structure containing organic substance, anhydrous minerals and icy materials. As revealed by recent spacecraft missions, aqueous altered materials were also detected [1,2]. Detection of these aqueous altered minerals suggest that comet nuclei once had liquid water. Post shock heat induced by impact may be one of the heat sources to induce liquid water because impact heating is highly effective on porous material [3,4]. Laboratory cratering experiments to measure the post shock temperature on porous H<sub>2</sub>O ice have been conducted for the study of comet nuclei [4]. Oblique impacts conducted on cohesive porous target suggests that the crater formation efficiency and the crater shape would be affected by impact angle [5]. However, the laboratory experiments for oblique impacts on ice is quite limited. Here we present the results on crater size, crater morphology and post shock heat on porous ice and discuss the effects of impact angle.

**Method:** Porous ice targets were prepared in a cold room (-15°C), controlling their porosity 40% using sieved grain crushed from ice cube. Post shock heat was measured using K-type thermocouples carefully placed in certain depths. Al-projectile ( $\phi=2$  mm) is propelled by two-stage light gas gun facility at ISAS. Impact experiments were conducted at impact velocities of  $v=3.0, 4.2, 6.0$  km/s, and at impact angles of  $\theta= 15^\circ, 30^\circ, 45^\circ$  (Fig.1). The target was placed in a vacuum ( $\sim 200$  Pa) chamber at room temperature just prior to the experiment ( $< 5$ min.) from a refrigerator (-20°C). The measured temperatures were recorded by a data logger with a sampling period of 10 ms.

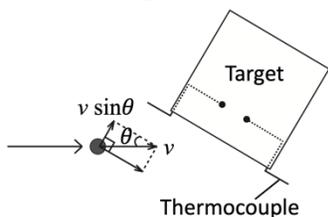


Fig.1 Impact angle.

### Result:

**Crater morphology.** Fig.2 is a photograph of the crater viewed from above. There is a refrozen layer on the crater wall, which appears black because it contains fine-grained projectile fragments. For comparison, a crater formed by a vertical impact ( $v=4.2$ km/s) is shown in Fig.3. A vertical impact crater is circular when viewed from above. On the other hand, oblique impact craters are not perfectly circular, but elliptical at low velocities and at low angles. At  $\theta = 45^\circ$  and  $30^\circ$ , the crater shape was circular with projections on the downrange side at  $v = 6$  km/s, but at  $\theta = 45^\circ$  and  $v = 4$

km/s, the crater grew fish-shaped, and at  $v = 3$  km/s it becomes elliptical. On the other hand, at  $\theta=15^\circ$ , the crater shape is already elliptical at  $v=6$  km/s. It was found that the smaller the collision angle, the faster the elliptical transition velocity.

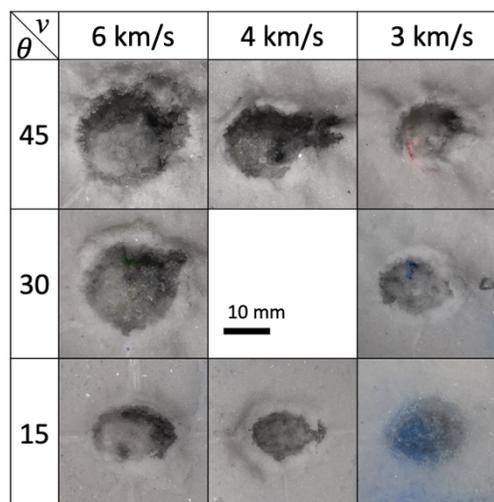


Fig.2 Impact craters formed by oblique impacts. The right side of each figure is the downrange side.



Fig.3 Impact crater formed by a vertical impact at  $v = 4.2$  km/s shown at the same scale as Fig.2.

**Crater size.** The crater size was studied by using the conventional crater scaling law to clarify the effects of oblique impacts on porous water ice (Fig.4 and 5). The  $\pi$  scaling law for crater size in the strength regime was used in this study. This  $\pi$  scaling law is written as follows [6],

$$\pi_R = H_1 \pi_Y^{-1/2} \pi_4^{1-3\nu/3},$$

where  $\pi_R$  and  $\pi_Y$  are nondimensional parameters described as follows,

$$\pi_R = R \left( \frac{\rho}{m} \right)^{1/3}, \pi_Y = \frac{Y}{\rho v_i^2} \text{ and } \pi_4 = \frac{\rho}{\delta^2},$$

where  $R$  is a crater radius,  $\rho$  is a target density,  $m$  is a projectile mass, and  $\delta$  is a projectile density. The target compressive strength  $Y$  for our 40% targets was assumed to be 628 KPa. The  $\mu$ ,  $\nu$  and  $H$  are constants depending on the material physical properties;  $\nu=0.4$  [6].

A bold line in Fig.4 and 5 is a fitted line of results for vertical impacts,  $\theta=90^\circ$ , expressed by the following equation:

$$\pi_R = 10^{-0.432 \pm 0.15} \pi_4^{-0.067} \pi_Y^{-0.203 \pm 0.032} [4].$$

For  $\pi_R$  in Fig.4, we used  $R$  of equivalent radius derived from measured area of ellipse shape crater for oblique impact. In Fig.4, at  $\theta=15^\circ$ , the crater is smaller than the scaling relationship and appears to be not scaled. To consider the effects of oblique impacts, we used  $R = R_{\text{minor}}$  measured in the manner shown in Fig.6, and  $v = v\sin\theta$  for  $\pi_Y$ . Thus, it is clear that this newly proposed  $\pi_Y'$  improved the relationship at all impact angles as shown in Fig.5.

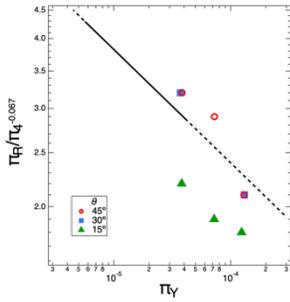


Fig.4  $\pi$ -scaling of crater radius.

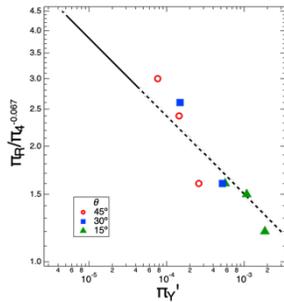


Fig.5  $\pi$ -scaling of crater radius considering the effect of oblique impact.

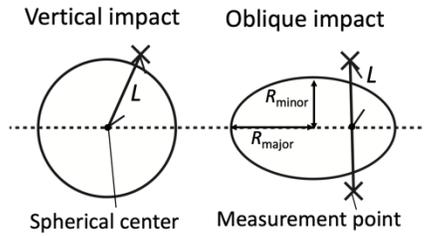


Fig.6 Distance  $L$  defined for circular and elliptical crater formed by vertical and oblique impacts, respectively.

*Post shock heat measurement.* Figure 7 shows the temperature change measured by a thermocouple at three different distances from the crater center of  $L=20, 21, 25$  mm. After the temperature rose and reached the maximum temperature, it gradually decreased. The smaller the distance  $L$  from the crater center, the larger the temperature rise and the faster the maximum temperature is reached. Therefore, it is considered that the heat induced by the impact was embedded in the crater wall, and then conducting into the target interior.

The maximum value of temperature change measured by a thermocouple is  $\Delta T_{\text{max}}$ , and the relationship between  $\Delta T_{\text{max}}$  and the normalized distance  $L/R$  (where  $R$  is the thermal diffusion distance) is shown in Fig.8. The thick line is the fitting line of the post shock temperature distribution due to vertical impact. In Fig.8, equivalent radius is used for  $R$  and  $L$  is the distance shown in Fig.6. The results for  $\theta=45^\circ$  are almost the same as our previous results shown as the fitted bold line for  $\theta=90^\circ$ . On the other hand, the data of  $\theta=30^\circ$  scatters around this line. The data of  $\theta=15^\circ$  is smaller than the resolution (0.1K) of our data logger,

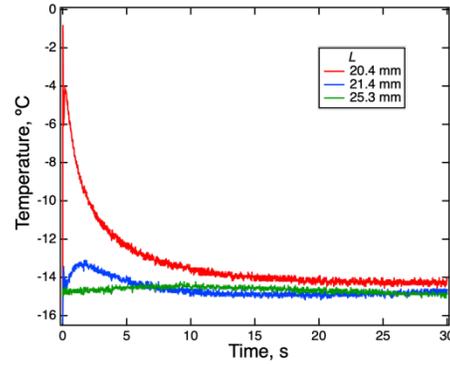


Fig.7 Temperature histories measured by thermocouples.

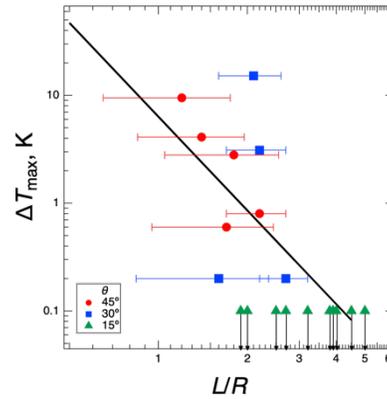


Fig.8 Distribution of  $\Delta T_{\text{max}}$ . Error bars show the value range.

and indicates that the temperature rise was smaller than the fitted line for  $\theta=90^\circ$ .

The reason why the temperature rises at  $\theta=30^\circ$  and  $15^\circ$  were lower than  $\theta = 90^\circ$  is assumed to be as follows. First, the crater depth was shallower at lower impact angles, the measurement points of the temperature was then farther from the crater wall. Second, the melt layer adjacent to the measurement point could be ejected away from the crater wall due to the effect of oblique impact. In addition, the reason why the temperature was high in the result of  $\theta = 30^\circ$  is considered as follows: There were places where the temperature was locally high due to the presence of local melt pockets under the crater wall.

**References:** [1] Altwegg et al. (2016), *Sci. Adv.* 2, e1600285; [2] Berger et al. (2011), *GCA* 75, 3501-3513; [3] Yasui et al. (2021) *Communications Earth & Environment*, 2, 95 [4] Sasai et al. (2021) *LPS LIV*, Abstract #1974. [5] Suzuki et al. (2021) *Planetary & Space. Sci.*, 195, 105141 [6] Housen & Holsapple et al. (2011) *Icarus*, 211, 856–875.